

Theoretical Study on Reaction Mechanism of Ground-State Cyano Radical with 1,3-Butadiene: Prospect of Pyridine Formation

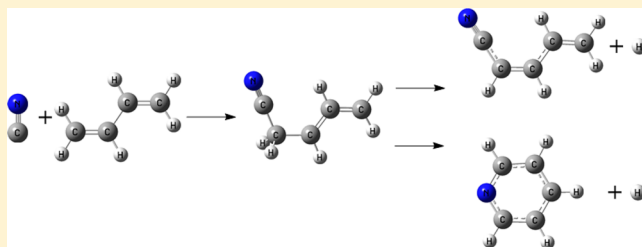
B. J. Sun,[†] C. H. Huang,[†] S. Y. Chen,[†] S. H. Chen,[†] R. I. Kaiser,[‡] and A. H. H. Chang*,[†]

[†]Department of Chemistry, National Dong Hwa University, No.1 Sec. 2 Da Hsueh Road, Shoufeng, Hualien 974, Taiwan

[‡]Department of Chemistry, University of Hawaii at Manoa, 2545 McCarthy Mall, Honolulu, Hawaii 96822, United States

S Supporting Information

ABSTRACT: The reaction of ground-state cyano radicals, $\text{CN}(\text{X}^2\Sigma^+)$, with the simplest polyene, 1,3-butadiene ($\text{C}_4\text{H}_6(\text{X}^1\text{A}_g)$), is investigated to explore probable routes and feasibility to form pyridine at ultralow temperatures. The isomerization and dissociation channels for each of the seven initial collision complexes are characterized by utilizing the unrestricted B3LYP/cc-pVTZ and the CCSD(T)/cc-pVTZ calculations. With facilitation of RRKM rate constants, through ab initio paths composed of 7 collision complexes, 331 intermediates, 62 hydrogen atom, 71 hydrogen molecule, and 3 hydrogen cyanide dissociated products, the most probable paths at collision energies up to 10 kcal/mol, and thus the reaction mechanism, are determined. Subsequently, the corresponding rate equations are solved that the concentration evolutions of collision complexes, intermediates, and products versus time are obtained. As a result, the final products and yields are determined. The low-energy routes for the formation of most thermodynamically stable product, pyridine, are identified. This study, however, predicts that seven collision complexes would produce predominately 1-cyano-1,3-butadiene, $\text{CH}_2\text{CHCHCHCN}$ (**p2**) plus atomic hydrogen via the collision complex **c1**($\text{CH}_2\text{CHCHCH}_2\text{CN}$) and intermediate **i2**($\text{CH}_2\text{CHCH}_2\text{CHCN}$), with a very minor amount of pyridine. Our scheme also effectively excludes the presence of 2-cyano-1,3-butadiene, which has energy near-degenerate to 1-cyano-1,3-butadiene, as supported by experimental findings.



I. INTRODUCTION

In the past decade, bimolecular reactions of the cyano radical ($\text{CN}; \text{X}^2\Sigma^+$) have emerged to play a significant role in the formation of nitriles—organic molecules carrying the CN group in the interstellar medium, hydrocarbon-rich atmospheres of planets and their moons such as Saturn's satellite Titan, and combustion. At temperatures as low as 13 K, cyano radicals react with unsaturated hydrocarbons without entrance barriers, of which rate constants are in a few $10^{-10} \text{ cm}^3 \text{s}^{-1}$ near gas kinetics limit as recent kinetics investigations demonstrated.^{1,2} Crossed molecular beam studies of reactions of cyano radical with acetylene,³ ethylene,⁴ benzene,⁵ allene,⁶ methylacetylene,⁷ and propylene,⁸ have identified CN and H exchange channels through CN insertion mechanism that readily result in the formation of various nitriles such as cyanoacetylene (HCCCN), vinylcyanide ($\text{C}_2\text{H}_3\text{CN}$), and methylcyanoacetylene (CH_3CCCN), for example. Ab initio electronic structure calculations are in support of the findings, although for propylene⁹ the major pathway is CH_3 dissociation with relatively minor H eliminations.

Although not detected, PAHs (polycyclic aromatic hydrocarbons) are long thought to exist in interstellar mediums¹⁰ and presumed to be responsible for certain unidentified infrared (UIR) bands¹¹ and the diffuse interstellar bands (DIBs).¹² The PAH building block, benzene (C_6H_6), is observed in protoplanetary nebula CRL 618,¹³ yet pyridine ($\text{C}_5\text{H}_5\text{N}$),

isoelectronic to benzene and unit of nitrogen-substituted PAHs (N-PAHs), has thus far eluded detection in extraterrestrial environments. Despite the prebiotic significance of N-PAHs, the formation mechanism of even the simplest N-PAHs is not well understood. Under condition of single-collision, the reaction of ethynyl radical (C_2H) and 1,3-butadiene (C_4H_6) was demonstrated¹⁴ to be capable of generating benzene without entrance barrier. It would be logical to access pyridine formation through a parallel reaction of 1,3-butadiene with CN, likewise isoelectronic to C_2H . While kinetics experiments monitor decay of the cyano radical and crossed molecular beam investigations sample products, electronic structure calculations could reveal the channels from reactants, intermediates, all the way to products. Hence an investigation combining kinetics studies, crossed molecular beam, and electronic structure calculation has been carried out to provide a comprehensive insight into the mechanism of $\text{CN} + 1,3\text{-butadiene}$ reaction.¹⁵

Here we conduct an extensive theoretical investigation of the reaction of the cyano radical with 1,3-butadiene to shed light if the aromatic pyridine molecule can indeed be formed under single collision conditions via a bimolecular reaction. A combined ab initio electronic structure and RRKM calculation

Received: June 8, 2014

Revised: August 6, 2014

Published: August 12, 2014



is presented to elucidate the reaction mechanism and to gauge the prospect of pyridine production for cyano radical and 1,3-butadiene reaction. The aim is to identify the kinetically competitive exoergic channels utilizing ab initio electronic structure calculations to then deduce the reaction mechanism by computing the RRKM rate constants under the condition of single binary-collision at various collision energies, to obtain concentration evolutions and thus lifetimes of the species involved by numerically solving the rate equations that correspond to the reaction mechanism, and to eventually estimate energy-dependent product branching ratios.

Similar schemes have successes in locating mainly the major products for the reactions of $C(^3P) + HC_4H$ (diacetylene),¹⁶ $C(^3P) + HC_6H$ (triacetylene),¹⁷ and $CN(X^2\Sigma^+) + C_3H_6$ (propylene).⁹ Potentially tracking a minor product, in this case, pyridine, the reaction channels would presumably branch out considerably compared with those including only major products, which poses a challenge to the computation and a test to our scheme.

II. THEORETICAL METHODS

1. Ab Initio Electronic Structure Calculations: Reaction Channels Prediction. The probable channels of the $CN(X^2\Sigma^+) + C_4H_6$ (X^1A_g) reaction are inferred by assuming that in single collision the reaction proceeds on the adiabatic doublet ground-state potential energy surface of C_5H_6N . The attack of electron deficient cyano radical on the π system of butadiene is anticipated to generate multiple collision complexes. Likely collision complexes are identified and their isomerization and dissociation channels are then characterized. The geometries for collision complexes, intermediates, transition states, and dissociation products are optimized along with the harmonic frequencies by employing the unrestricted B3LYP^{18–21}/cc-pVTZ calculations. With unrestricted B3LYP/cc-pVTZ zero-point energy corrections, the coupled cluster^{22–25} CCSD(T)/cc-pVTZ energies are further computed. Note that although complete basis set CCSD(T)/CBS limit was considered for selected species in ref 15, it is not done in the present work. The transition-state structures are determined by examining the vibrational mode with imaginary frequency being the reaction coordinate in question. IRC (intrinsic reaction coordinate) calculations are carried out only when ambiguity arises. The electronic structure calculations are performed by utilizing the Gaussian 98 and 03 programs.²⁶

2. RRKM Theory: Energy-Dependent Rate Constants. According to the RRKM theory, when the total energy is constant and equilibrated among internal degrees of freedom throughout the reaction, $A^* \xrightarrow{k} A^\ddagger \rightarrow P$, in which A^* is the energized reactant, A^\ddagger is the transition state, and P is the product, the energy-dependent rate constant $k(E)$ is expressed as²⁷

$$k(E) = \frac{\sigma}{h} \frac{W^\ddagger(E - E^\ddagger)}{\rho(E)} \quad (1)$$

where σ is the symmetry factor, W^\ddagger the number of states of the transition state, E^\ddagger the transition-state energy, and ρ is the density of states of the reactant. In general, the number of states $W(E)$ and density of state $\rho(E)$ are related to partition function $Q(\beta)$ as²⁸

$$W(E) = \frac{1}{2\pi i} \int_c \frac{d\beta}{\beta} e^{\beta E} Q(\beta) \quad (2)$$

$$\rho(E) = \frac{1}{2\pi i} \int_c e^{\beta E} Q(\beta) d\beta \quad (3)$$

In our work, the molecule is treated as a collection of harmonic oscillators that only the vibrations are considered for $Q(\beta)$, and the tunnel effect is not incorporated. ρ and W^\ddagger are computed based on saddle-point method,^{27,28} and the energies and harmonic frequencies evaluated as in Section 1 are utilized.

3. Rate Equation Solutions: Concentration Evolutions and Branching Ratios. For each collision complex, the Runge–Kutta method is used to solve the rate equations of reaction mechanism at 0 and 10 kcal/mol. In addition, for complex **c1**, the equations are also solved at 6.2 kcal/mol. The solutions give the concentrations of species as a function of time. The asymptotic values yield the final branching ratio.

III. RESULTS AND DISCUSSION

The barrierless addition of CN to the π system of butadiene initiates the reaction. Each effective collision of the reactants could produce one collision complex. CN can attack 1,3-butadiene through either carbon or nitrogen; the collision complex could be acyclic or cyclic, and when the latter is formed, both three- and four-member rings are likely. All probable eight-collision complexes are found and denoted as **c1–c8**; the B3LYP/cc-pVTZ optimized geometries are plotted in Figure 1.

The reaction paths of each collision complex are assembled independently, except for **c8** due to its higher than reactant's energy that results from both three-member ring strain and reacting via nitrogen of CN. Note that the more stable conformation, *trans*-1,3-butadiene, is assumed for reactant. IRC calculations at the B3LYP/cc-pVTZ level along the breaking C–CN bond are performed for **c1**, which supports the barrierless formation. The immediate isomerization channels of **c1–c7** bound relative to reactants are characterized, which include hydrogen shift, CN shift, ring formation, ring opening, and hydrogen atom elimination. Subsequently, the rate constants are computed for the paths under 10 kcal/mol. To avoid escalating the number of paths to be computed, only the immediate channels of the largest rate constants, or the most kinetically competitive pathways are further tracked. The reaction paths would no longer be pursued when a dissociation occurred.

The energetic paths of **c1–c7** are illustrated in Figures 2–8. Their reaction mechanisms at collision energy of 0–10 kcal/mol are collected in Figure 9. The geometries of intermediates, dissociation products, and transition states optimized with B3LYP/cc-PVTZ are named **i**, **p**, and **ts** and shown, respectively, in Figures s1–s3 in the Supporting Information. The energies are listed in Table s1 in the Supporting Information, and the rate constants at collision energies of 0.0, 0.03, 0.15, 2.0, 5, 6.2, and 10 kcal/mol are compiled in Table s2 in the Supporting Information.

If not stated otherwise, the energies discussed are the CCSD(T)/cc-pVTZ energies with B3LYP/cc-pVTZ zero-point energy corrections, and the rate constants at zero collision energy are cited.

1. Most Probable Paths of Collision Complex **c1.** Ring formation in general encounters lower barrier than the isomerization involved bond breaking. For the most stable complex **c1** located at –61.5 kcal/mol, an acyclic species with CN connected to the terminal C of C_4H_6 , as seen in Figure 2, there could be 15 low energy channels including the

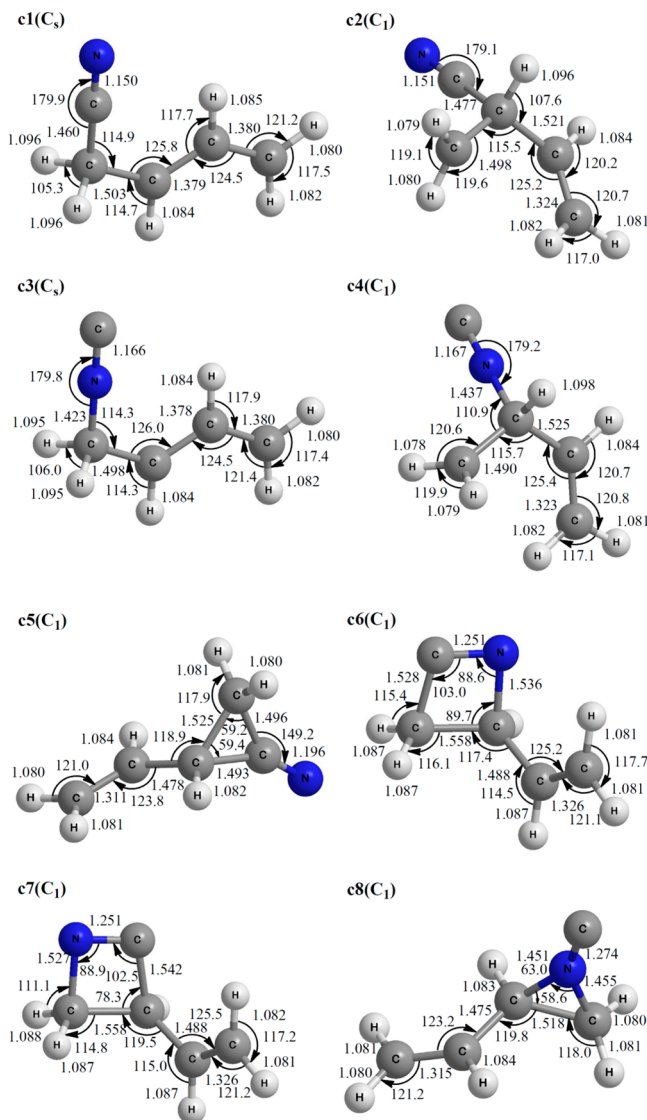


Figure 1. B3LYP/cc-pVTZ optimized geometries of the eight collision complexes of the $\text{CN}(^2\Sigma^+)$ + 1,3-butadiene(${}^1\text{A}_g$) reaction, in which the point group is in parentheses, lengths are in angstroms, and angles are in degrees.

dissociation back to reactants. Among them, the five-member-ring closure of $\text{c}1 \rightarrow \text{i}1$ is the fastest as indicated by its RRKM rate constant k_1 ($3.74 \times 10^{10} \text{ s}^{-1}$) at zero collision energy being three orders of magnitude larger than the second in line k_3 of $\text{c}1 \rightarrow \text{c}5$, a three-member-ring formation.

The channels of kinetically competitive $\text{i}1$ are traced further as detailed in Figure s4 in the Supporting Information, which demonstrates that the only option at low energy is a reversed ring-opening back to $\text{c}1$. $\text{c}1$ would look for the next probable path, to three-member-ringed $\text{c}5$, for dissipation of its concentration buildup, which, however, as discussed later eventually turns $\text{c}1$. The third fastest channel for $\text{c}1$ is likewise a ring-formation to $\text{i}3$ with six-member-ring. $\text{i}3$ also prefers a ring-opening to $\text{c}1$ instead of breaking the ring to become $\text{c}3$, as analyzed in Figure s5 in the Supporting Information. Subsequently, through 1,2 H shift, $\text{c}1$ converts to $\text{i}2$, with k_4 being $1.59 \times 10^6 \text{ s}^{-1}$. The probable paths of $\text{i}2$ examined in Figure s6 in the Supporting Information indicate that it favors a ring-closure to $\text{i}11$, which could open the ring to $\text{c}2$ eventually

arriving at $\text{c}1$, as discussed later. Finally, in the single-collision environment, $\text{c}1$ completes or ends the reaction via the fifth most probable channel of dissociating a hydrogen atom from the terminal carbon to generate $\text{p}2$, 1-cyano-1,3-butadiene. The most probable paths of $\text{c}1$ thus derived are marked red in Figure 2. The dominate product, $\text{p}2$, seemingly makes $\text{CN} + \text{C}_4\text{H}_6$ a simple CN substituting H reaction.

2. Most Probable Paths of Collision Complex $\text{c}2$.

Within 11 low-energy paths identified for $\text{c}2$ in Figure 3, rate constant calculations predict three-member-ring formation that leads to $\text{i}11$ is most likely because k_{21} ($\text{c}2 \rightarrow \text{i}11$) is 70 times the second largest, k_{20} , to $\text{c}5$ also with a three-member-ring. The likely outcome of $\text{i}11$ is further scrutinized in Figure s6 in the Supporting Information. It reveals that $\text{i}11$ would soon break the ring to $\text{i}2$, which shoots right back at $\text{i}11$; the more practical way out for $\text{i}11$ is returning to $\text{c}2$, judging from the ratio of k_{-21} ($\text{i}11 \rightarrow \text{c}2$) and k_{-29} ($\text{i}11 \rightarrow \text{i}2$) that gives a decent 0.15. Therefore, for $\text{c}2$, the completion of the title reaction is then a conversion to $\text{c}5$, which easily isomerizes into $\text{c}1$ and assumes the paths of the latter, as discussed later.

3. Most Probable Paths of Collision Complex $\text{c}3$.

As seen in Figure 4, cyclization and H shift produce eight isomerization channels for $\text{c}3$, 1-isocyano-1,3-butadiene. Similar to $\text{c}1$ and $\text{c}2$, the paths with the lowest barriers are six-member ($\text{i}3$), five-member ($\text{i}28$), and four-member ($\text{c}7$) ring closure, in descending rate (constant). These are also the only pathways with transition states in negative energy. k_{14} ($\text{c}3 \rightarrow \text{i}3$) overwhelms the other two, k_{17} ($\text{c}3 \rightarrow \text{i}28$) and k_{18} ($\text{c}3 \rightarrow \text{c}7$), by almost five orders, as listed in Table sII in the Supporting Information. Figure s5 in the Supporting Information illustrates that once $\text{i}3$ is generated, ~1% of $\text{i}3$ goes back to $\text{c}3$, 99% ring-opens to $\text{c}1$, and it is practically zero chance for other intermediates to be present, giving k_{-14} ($\text{i}3 \rightarrow \text{c}3$)/ k_{-2} ($\text{i}3 \rightarrow \text{c}1$) ≈ 0.01 and others/ k_{-2} ≈ 0 . That is, the isocyano compound $\text{c}3$ converts to its cyano counterpart, $\text{c}1$, by way of a six-member ring-closure and -opening.

4. Most Probable Paths of Collision Complex $\text{c}4$. It is clear from Figure 5 that the only channel open for $\text{c}4$ at zero collision energy is the formation of three-member ringed $\text{i}52$. As detailed in Figure s7 in the Supporting Information, $\text{i}52$ chooses a five-member ring closure ($\text{i}20$), then breaks the newly formed ring to become $\text{i}9$, which opens the remaining three-member ring to $\text{c}1$.

5. Most Probable Paths of Collision Complexes $\text{c}5$, $\text{c}6$, and $\text{c}7$.

For the ringed complexes, $\text{c}5$, $\text{c}6$, and $\text{c}7$, strategic ring-openings to the acyclic complexes are shown to be minimum energy paths, as presented in Figures 6–8, respectively, and proven to be the most probable in Table sII in the Supporting Information. At zero energy, $\text{c}6 \rightarrow \text{c}1$ and $\text{c}7 \rightarrow \text{c}3$ are the exclusive outcomes for $\text{c}6$ and $\text{c}7$, while $\text{c}5$ transforms into $\text{c}1$ and $\text{c}2$ with a ratio of 3 to 1, as estimated from k_{-3} ($\text{c}5 \rightarrow \text{c}1$)/ k_{-20} ($\text{c}5 \rightarrow \text{c}2$) in Table sII in the Supporting Information.

6. Reaction Mechanisms. The most probable paths of $\text{c}1$ – $\text{c}7$ in Figures 2–8 are found to persist even when collision energy rises to 10 kcal/mol. The most probable paths inferring reaction mechanisms are laid out in Figure 9. Figure 9, which emphasizes the directions of reaction instead of energetic aspect, clearly demonstrates that all complexes eventually convert to the most stable $\text{c}1$, specifically, acyclic $\text{c}2$, $\text{c}3$, and $\text{c}4$, through first ring-formation while the cyclic $\text{c}5$, $\text{c}6$, and $\text{c}7$ convert via ring-opening. It thus firmly establishes that the major product is $\text{p}2 + \text{H}$.

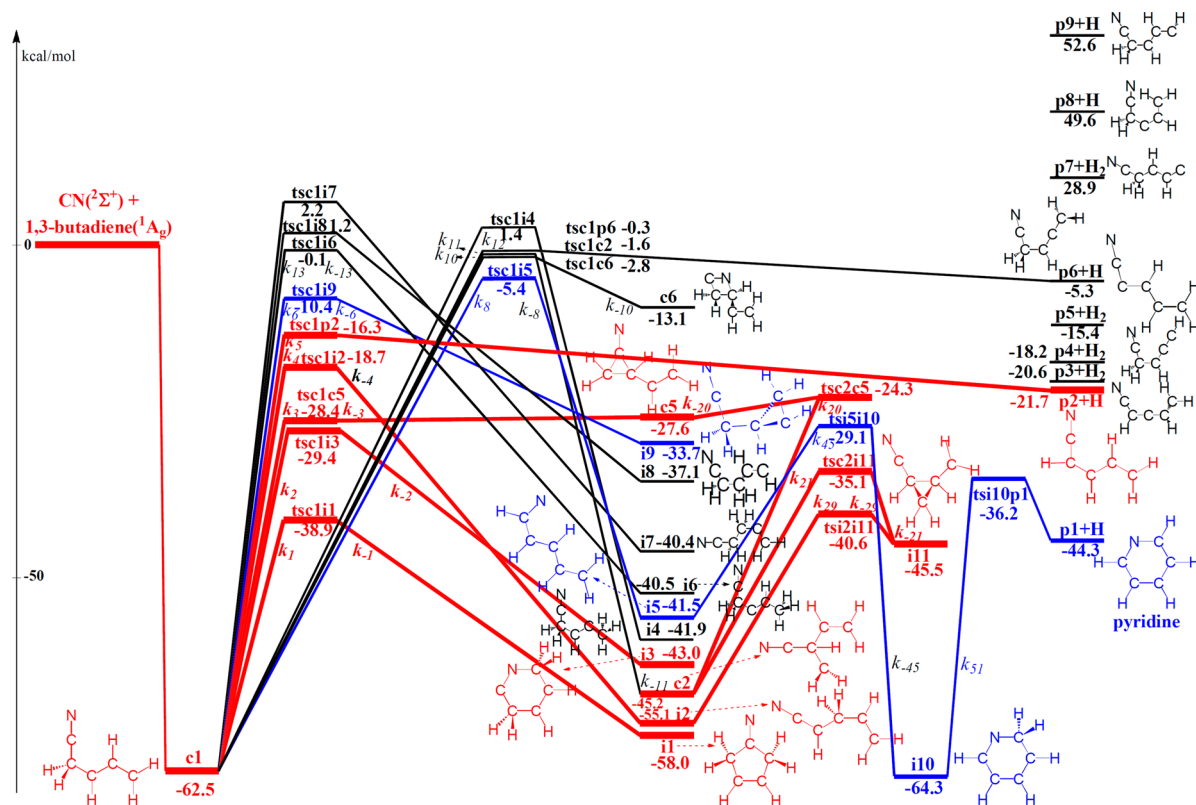


Figure 2. Reaction paths and the most probable paths (highlighted in red) at 0–10 kcal/mol collision energy of the collision complex, c1, in which the energies are computed at the CCSD(T)/cc-pVTZ level of theory with B3LYP/cc-pVTZ zero-point energy corrections at the B3LYP/cc-pVTZ optimized geometries. Note for c1 dissociation products, p3–p5 and p7–p9, the attempts are not made in locating the transition states.

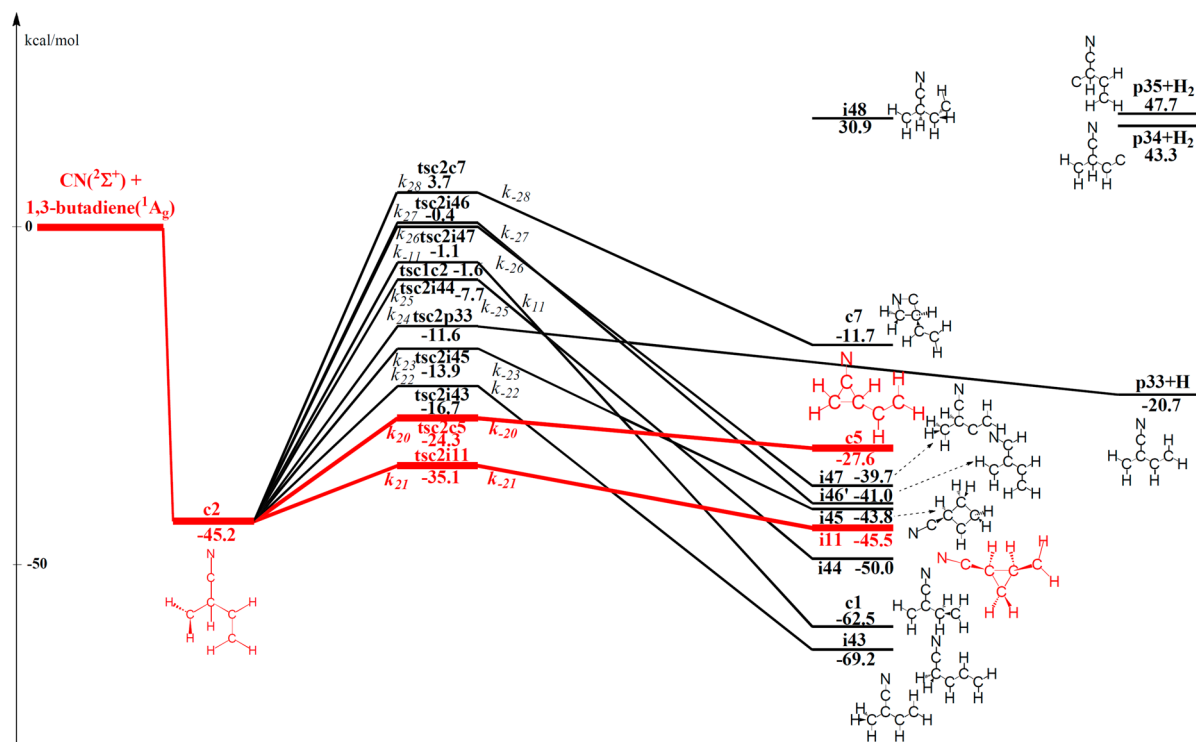


Figure 3. Reaction paths and the most probable paths (highlighted) at 0–10 kcal/mol collision energy of the collision complex, **c2**, in which the energies are computed at the CCSD(T)/cc-pVTZ level of theory with B3LYP/cc-pVTZ zero-point energy corrections at the B3LYP/cc-pVTZ optimized geometries. Note for **c2** intermediate, **i48**, and dissociation products, **p34** and **p35**, the attempts are not made in locating the transition states.

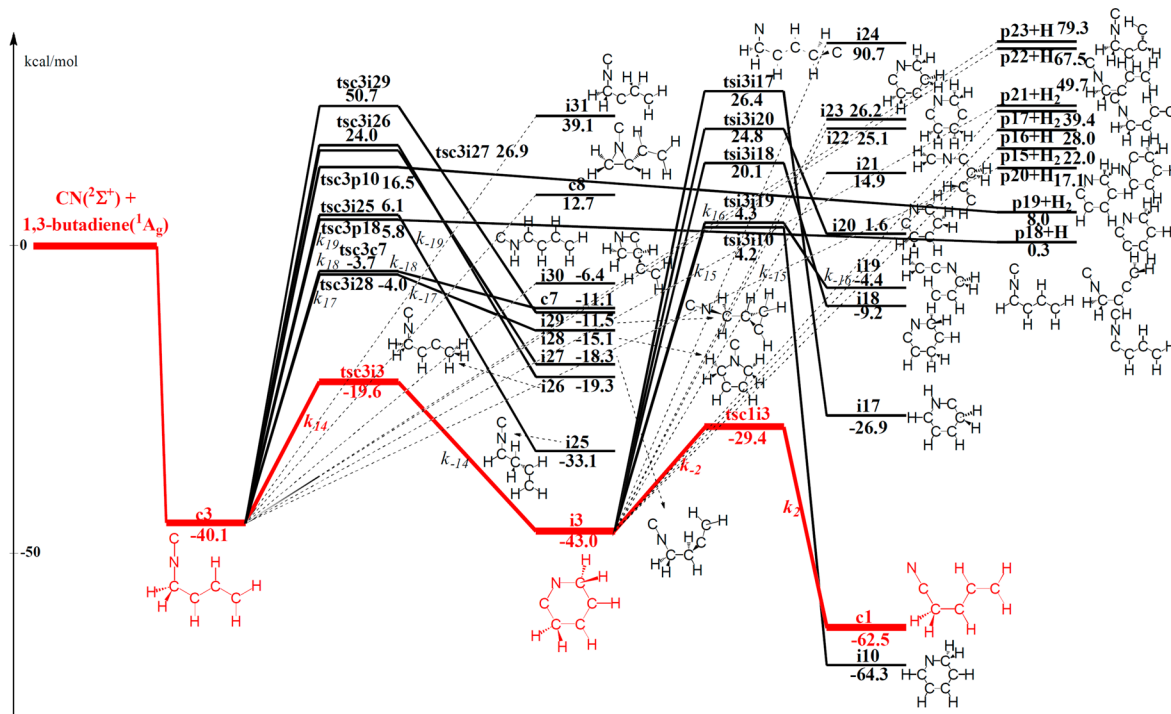


Figure 4. Reaction paths and the most probable paths (highlighted) at 0–10 kcal/mol collision energy of the collision complex, **c3**, in which the energies are computed at the CCSD(T)/cc-pVTZ level of theory with B3LYP/cc-pVTZ zero-point energy corrections at the B3LYP/cc-pVTZ optimized geometries. Note for those paths in dotted lines the attempts are not made or not successful in locating the transition states.

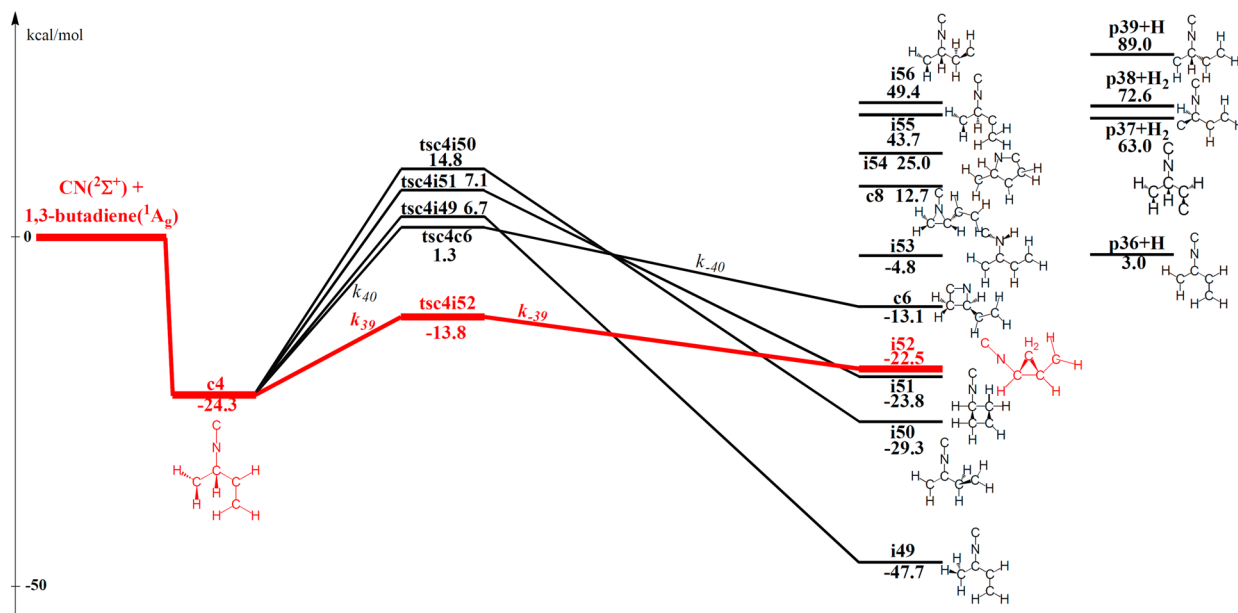


Figure 5. Reaction paths and the most probable paths (highlighted) at 0–10 kcal/mol collision energy of the collision complex, **c4**, in which the energies are computed at the CCSD(T)/cc-pVTZ level of theory with B3LYP/cc-pVTZ zero-point energy corrections at the B3LYP/cc-pVTZ optimized geometries. Note for **c4** intermediates, **i53–i56**, **c8**, and dissociation products, **p36–p39**, the attempts are not made in locating the transition states.

7. Concentration Evolution and Lifetime. By adopting the RRKM rate constants in Table sII in the Supporting Information, the rate equations of reaction mechanisms in Figure 9a–g are solved numerically. Namely, these are seven sets of simultaneous differential equations in 8, 8, 9, 13, 8, 9, and 10 unknown concentrations, respectively. At zero collision energy, the solutions, evolution of concentrations with time, for

c1 reaction mechanism are presented in Figure 10, and those of **c2–c7** are in Figure s8 in the Supporting Information.

Zero Collision Energy. Figure 10 demonstrates when the reaction proceeds via **c1**, with the concentration being 1 initially, **c1** decays as intermediates peak and disappear, and the only product **p2** reaches the asymptotic value 1. The peak concentrations of the intermediates, **i1**, **i3**, **i2**, **i11**, and **c2**, precisely duplicate the predictions of the steady-state

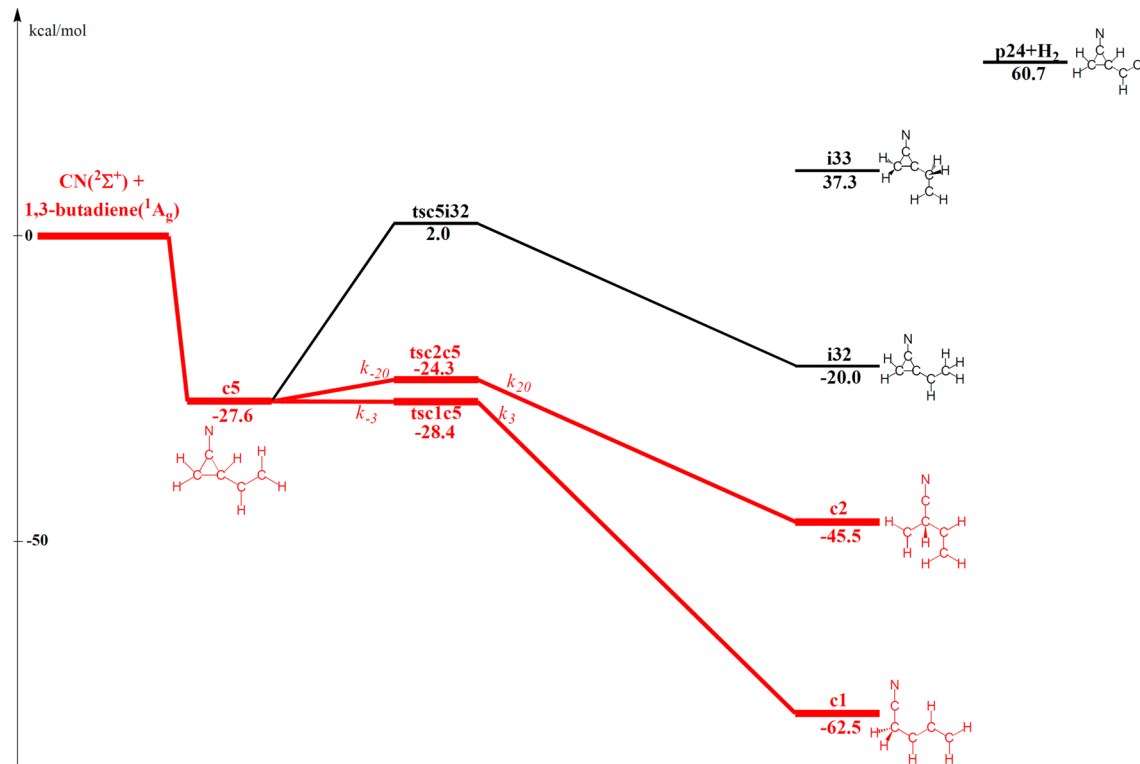


Figure 6. Reaction paths and the most probable paths (highlighted) at 0–10 kcal/mol collision energy of the collision complex, **c5**, in which the energies are computed at the CCSD(T)/cc-pVTZ level of theory with B3LYP/cc-pVTZ zero-point energy corrections at the B3LYP/cc-pVTZ optimized geometries. Note for **c5** intermediate, **i33**, and dissociation product, **p24**, the attempts are not made in locating the transition states.

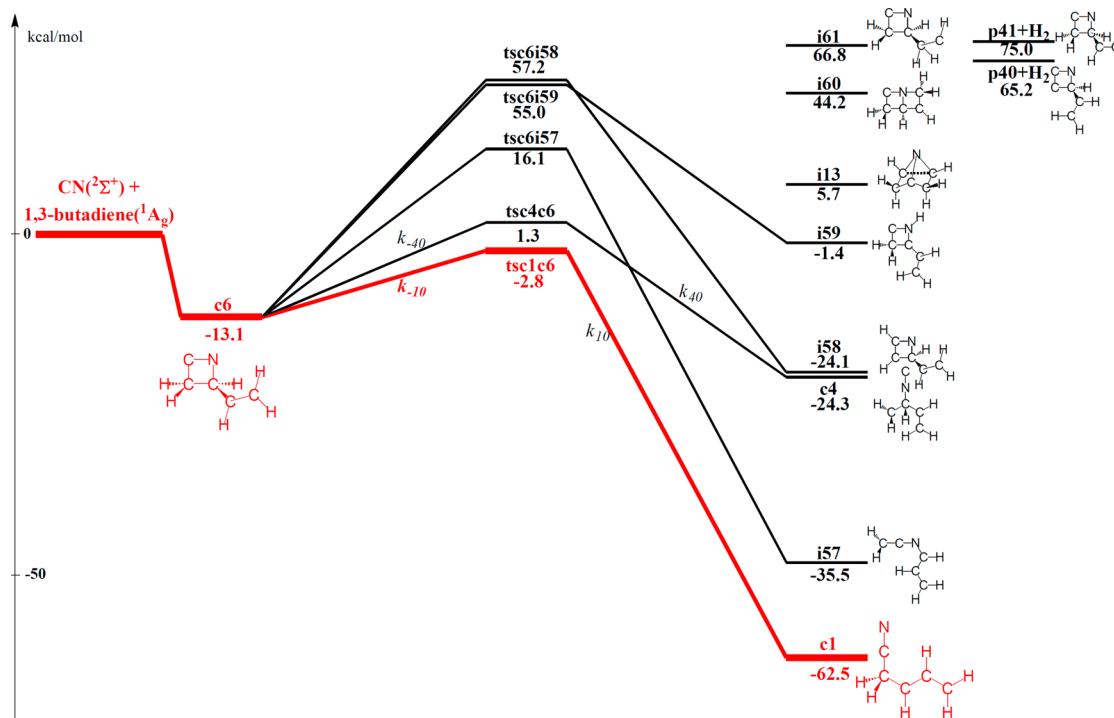


Figure 7. Reaction paths and the most probable paths (highlighted) at 0–10 kcal/mol collision energy of the collision complex, **c6**, in which the energies are computed at the CCSD(T)/cc-pVTZ level of theory with B3LYP/cc-pVTZ zero-point energy corrections at the B3LYP/cc-pVTZ optimized geometries. Note for **c6** intermediates, **i13**, **i60**, **i61**, and dissociation products, **p40**, **p41**, the attempts are not made in locating the transition states.

approximation, with an exception for **c5**, whose concentration is slightly off. For instance, on the basis of the steady-state approximation, at steady state the concentration of **i2** ought to

follow a relation of $[i2] = k_4[c1] + k_{-29}[i11]/[k_{29}]$ according to the mechanism in Figure 9a. Knowing the peak concentrations of **c1** and **i11** being 1 and 2.79×10^{-3} , respectively, the

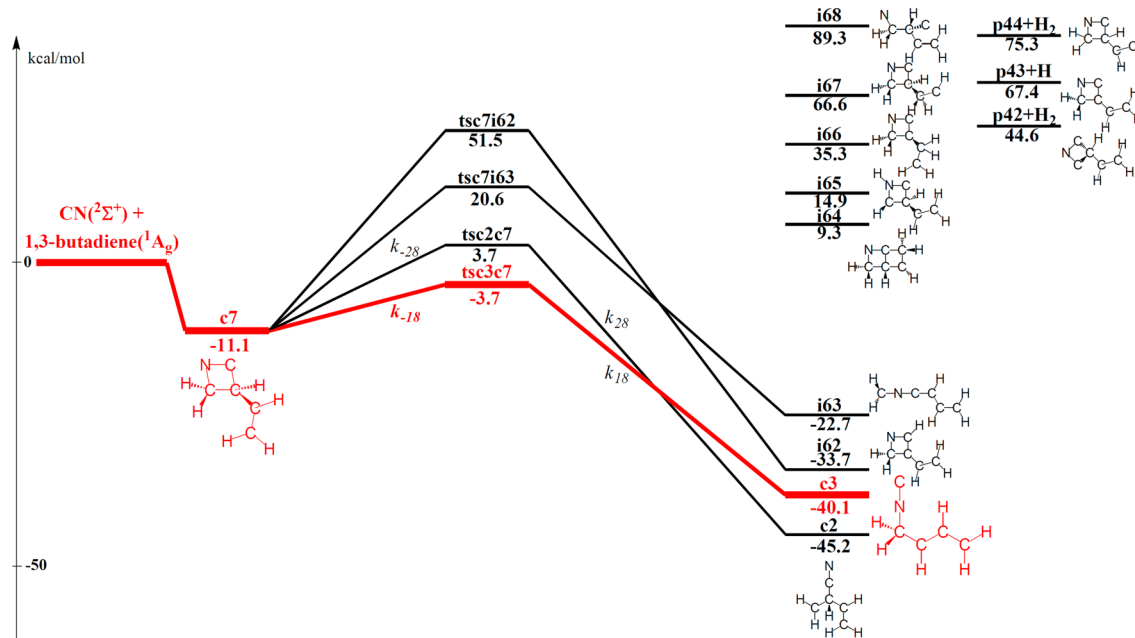


Figure 8. Reaction paths and the most probable paths (highlighted) at 0–10 kcal/mol collision energy of the collision complex, **c7**, in which the energies are computed at the CCSD(T)/cc-pVTZ level of theory with B3LYP/cc-pVTZ zero-point energy corrections at the B3LYP/cc-pVTZ optimized geometries. Note for **c7** intermediates, **i64–i68**, and dissociation products, **p42–p44**, the attempts are not made in locating the transition states.

equation yields the **i2** steady-state concentration, 0.244, which reproduces exactly the **i2** peak concentration noted in Figure 10.

Only **c1**, **i2**, and of course product **p2** amount to a healthy, 1, 0.244, and 1, respectively, and add up to almost 1 in the course of reaction, while the concentrations of others are dismal all the way. The **c1** lifetime reflects the magnitude of bottleneck rate constant k_5 of **c1** → **p2** + H, and likewise it takes the same order of microsecond to complete **p2** formation.

10 kcal/mol Collision Energy. With the RRKM rate constants at 10 kcal/mol in Table sII, Figure s9 in the Supporting Information gives the concentration evolutions for **c1–c7**. Specifically, for **c1** mechanism the intermediate concentrations peak higher and earlier than when the reaction proceeds at zero collision energy, and similarly, the peak concentrations replicate steady-state prediction.

Implication for Laboratory Detection. The barrierless **c1** formation is supported by our IRC calculations, which implies that the title reaction rate is gas-kinetics as the low-temperature kinetics study has shown.¹⁵ The concentration evolutions at 0 and 10 kcal/mol indicate that long-lived complex **c1** and **i2** could be detected a submicrosecond into the reaction. Within microseconds, a typical time scale for crossed beam experiment, the observed molecule would be 1-cyano-1,3-butadiene (**p2**) exclusively, a H loss from the terminal carbon attacked by CN. This terminal H loss is readily confirmed by crossed-beam experiments with partially deuterated 1,3-butadiene.¹⁵

It is noted that in Figure 3 a direct H dissociation from the second carbon of **c2** would generate 2-cyano-1,3-butadiene (**p33**), a mere 1 kcal/mol higher than 1-cyano-1,3-butadiene (**p2**). Electronic structure or potential energy surface calculations are not able to predict the outcome between the two products. Our scheme combining electronic structure, RRKM calculations, and rate equation solutions concludes the product is predominately **p2**, and the near degenerate **p33** would not be present.

8. Pyridine Formation. Formation Mechanism. While the predicted dominant products, **p2** + H, are of −21.7 kcal/mol in energy, the dissociation product of the lowest energy is in fact pyridine (**p1**) + H, the unit of nitrogen-substituted PAHs located at −44.3 kcal/mol. It is of great interest to resolve the pathways of pyridine formation and furthermore its yield. In the same vein of deducing the most probable or major products, the most probable paths are expanded to include the channels in the order of decreasing rate constants until the minor product, pyridine, is attained.

Because **c1** is the crucial collision complex, as interpreted further in Figure 2, in search of pyridine via **c1** the path following the last step **c1** → **p2** that concludes the most probable paths (red) would be **c1** → **i9**. The three-member ringed **i9** is most likely back to **c1** knowing its prospect, k_{-6} (**i9** → **c1**) / k_{44} (**i9** → **i20**), is ~100, as given in Figure s7 and Table sII in the Supporting Information. Guided by decreasing rate constant, **c1** subsequently H shifts to **i5**, which is examined in Figure s10 in the Supporting Information, and undergoes a six-member ring closure (**i10**). Finally, Figures s10 and s11 in the Supporting Information show that through dissociating a H atom **i10** promptly arrives at pyridine.

The pyridine formation paths thus determined are sketched (red and blue) in Figures 2 and 11. Note that for the paths from **i5** to pyridine only the swiftest channels are kept, which presumably would provide an upper bound for the yield of pyridine.

Branching Ratio. The rate equations for pyridine formation via **c1** are solved at 0, 6.2, and 10 kcal/mol to assess the energy-dependent branching ratio. As the concentration evolution elucidated in Figure s12 in the Supporting Information, the yield of **pyridine** (**p1**) is 0.005, 0.036, and 0.072% at collision energy of 0, 6.2, and 10 kcal/mol, respectively. It precisely coincides with k_8 (**c1** → **i5**) / k_5 (**c1** → **p2**) at 0, 6.2, and 10 kcal/mol, listed in Table sII in the Supporting Information. That is, as seen in Figure 2, the largest energy barrier for **c1** to

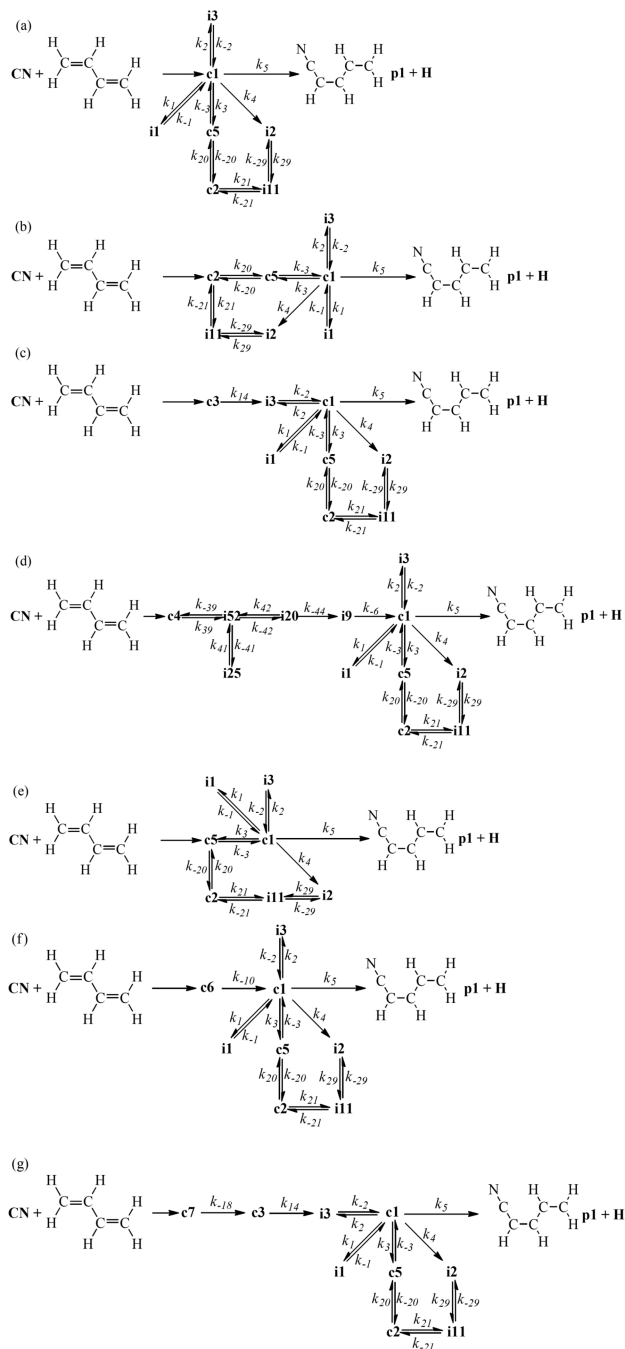


Figure 9. Reaction mechanisms a–g derived from the most probable paths of **c1**–**c7**, respectively, at 0–10 kcal/mol collision energy, where the k values are the corresponding rate constants.

eventually form **pyridine** is **c1** → **i5**, the rate-determining step of pyridine formation, which makes the branching, **pyridine**:**p2**, simply be **c1** → **i5**:**c1** → **p2**. Although pyridine yield is increasing with collision energy, the amount remains very minor as **p2** stays overwhelming. Raising the collision energy should facilitate the detection of pyridine. The extrapolation of k_8 / k_5 to 20 kcal/mol gives 0.235%.

Tunnel effect is not included. In general, the tunnel effect is important when the hydrogen atom is involved along the reaction coordinate, and the collision energy is near the energy barrier. **tsc1p2** located at −16.5 kcal/mol is a direct hydrogen atom loss, and tunnel effect is expected to enhance its rate

constant, k_5 , however, not as much as k_8 for **tsc1i5** of −5.4 kcal/mol, and likewise a H shift, a direct hydrogen atom involvement. Thus, the predicted yield of pyridine should rise, though not significantly, if tunneling is incorporated in RRKM calculations.

Comparison with Benzene Formation. In brief, for the acyclic **c1** to generate the cyclic pyridine, it requires (a) a H shift to the carbon of CN and (b) a six-member ring formation, and then surely a H dissociation. As seen in Figure 2, the energy barrier of the channel **c1**–(a) **i5**–(b) **i10**–pyridine; that is, **c1** → **i5** is 11 kcal/mol higher than the one for **c1** → **p2**, which results in very minor **pyridine** production. While in the $C_2H + 1,3$ -butadiene reaction,¹⁴ its **c1** analogous takes a route of (b)–(a)–benzene with a barrier 20 kcal/mol lower than that for acyclic **p2** counterpart formation, which would yield 40% benzene at zero collision energy.

9. Hydrogen Abstraction. With C_{2h} symmetry, there are three nonequivalent groups of hydrogen in 1,3-butadiene. Hydrogen abstraction by CN brings three products: $HCN + p64$, $HCN + p65$, and $HCN + p66$ are located. As expected, Figure s13 in the Supporting Information shows the barrier height is similar to $CN + propylene$,⁹ ~2 kcal/mol. While often neglected in the investigation for reaction of cyano with unsaturated hydrocarbons, Estillore et al.²⁹ have observed the H-abstraction channels for the $CN + 1$ -pentene reaction with crossed-beam imaging.

10. Species on C_5H_6N Potential Energy Surface. The number of relevant C_5H_6N isomers identified in the present work elevates to 331, and considering the $CN + C_3H_6$ (propylene) reaction,⁹ only 45 are utilized. Certainly, one more atom in the system contributes to the increasing number; however, the expansion of the reaction mechanism to accommodate the formation of a minor product, pyridine, advances the difficulty of the task considerably. It is also noted that the expectation values of S^2 ($= S(S+1)$) for all of the doublet ($S = 1/2$) species in the reaction mechanism of Figures 9 and 11 are practically 0.75 for both B3LYP/cc-pVTZ and CCSD(T)/cc-pVTZ, except for **i10**, whose S^2 is 0.86 in CCSD(T) calculation but still does not deviate too much from the doublet spin.

IV. CONCLUSIONS

The prospect of pyridine synthesis via the reaction of CN radical and 1,3-butadiene has been studied by combining ab initio electronic structure calculations and RRKM theory. The most probable paths are obtained by navigation of the RRKM rate constants through ab initio channels that are composed of 7 collision complexes, 331 intermediates, 62 H^- , 71 H_2^- , and 3 HCN-dissociated products, and the transition states. The reaction mechanisms then adopt the most probable paths that are reduced to around eight species at collision energies of 0, 6.2, and 10 kcal/mol. Concentration evolutions are obtained as the solutions of the rate equations for the reaction mechanisms. The reaction mechanism is extended to 12 species to assess pyridine formation for **c1** complex.

With CN addition to seven different positions in 1,3-butadiene, this investigation predicts that all seven collision complexes end up at one major product, the acyclic 1-cyano-1,3-butadiene (**p2**) + H, in agreement with experiments.¹⁵ The branching ratio of the most thermodynamically stable **pyridine** is estimated 0.005 to 0.072% at 0–10 kcal/mol and extrapolated to 0.235% even at 20 kcal/mol. Our study indicates that the barrierless and exoergic $CN + 1,3$ -butadiene

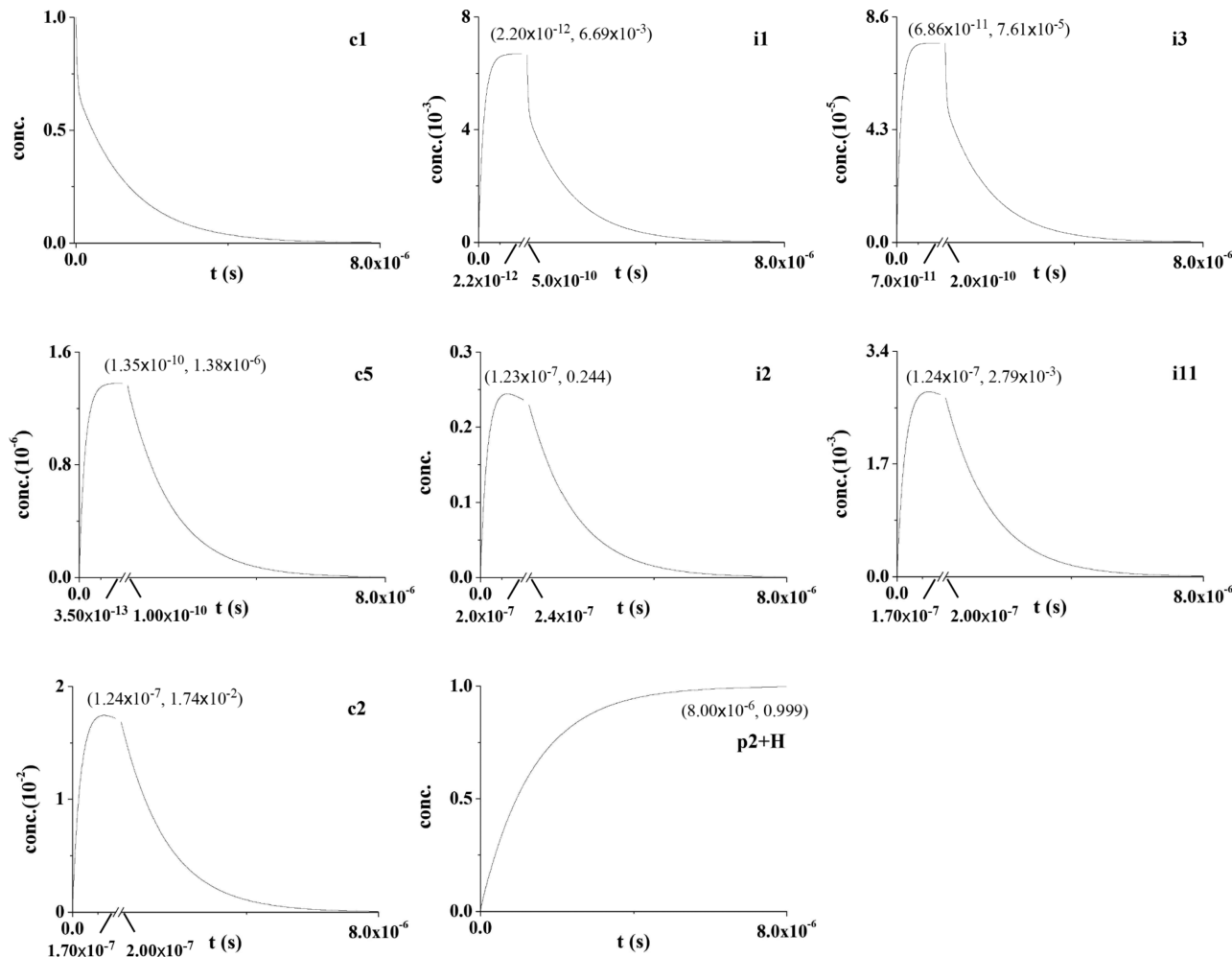


Figure 10. Concentration evolution for each species in **c1** reaction mechanism at 0 kcal/mol collision energy as in Figure 9

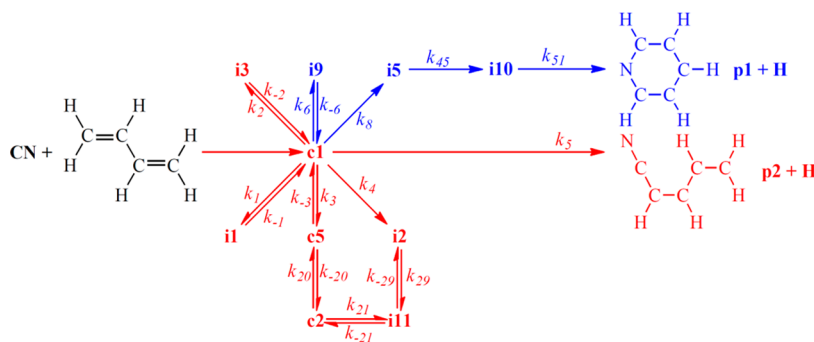


Figure 11. Reaction mechanism derived from the pyridine formation paths of **c1** at 0–10 kcal/mol collision energies.

reaction would be efficient for 1-cyano-1,3-butadiene formation in interstellar medium, with **pyridine** being the less prominent product.

The IRC calculation of **c1** back to reactants supports its barrierless formation, which is consistent with the rate coefficients of the overall reaction being close to gas kinetic limit, as demonstrated by low-temperature kinetics experiments.¹⁵ While electronic structure or potential energy surface calculations alone are not able to predict the outcome between near degenerate 1-cyano-1,3-butadiene (**p2**) and 2-cyano 1,3-butadiene (**p33**), our scheme of combining electronic structure, RRKM calculations, and rate equation solutions agrees with

crossed molecular beam experiments¹⁵ and concludes that product is exclusively **p2** due to atomic hydrogen loss from a terminal carbon. The investigation indicates that the present scheme would be effective in identifying major products and also predicting minor products in general, such as **p2** and **pyridine**, respectively, for titled reaction.

■ ASSOCIATED CONTENT

S Supporting Information

Computed energies, RRKM rate constants, and optimized geometries of intermediates; optimized geometries of products and transition states; reaction paths of **i1**, **i2**, **i3**, **i52**; evolution

of concentration for **c1–c7** at 0 and 10 kcal/mol; paths of **i5** and **i10**; evolution of concentration for pyridine formation at 0, 6.2, 10 kcal/mol; and hydrogen abstraction channels. This material is available free of charge via the Internet at <http://pubs.acs.org>.

AUTHOR INFORMATION

Corresponding Author

*E-mail: hhchang@mail.ndhu.edu.tw. Fax: +886-3-8633570.

Notes

The authors declare no competing financial interest.

ACKNOWLEDGMENTS

Computer resources at the National Center for High-performance Computer of Taiwan were utilized in the calculations.

REFERENCES

- (1) Carty, D.; Page, V. L.; Sims, I. R.; Smith, I. W. M. Low Temperature Rate Coefficients for the Reactions of CN and C_2H Radicals with Allene ($CH_2=CC=CH_2$) and Methyl Acetylene ($CH_3C\equiv CH$). *Chem. Phys. Lett.* **2001**, *344*, 310–316.
- (2) Hoobler, R. J.; Leone, S. R. Low-Temperature Rate Coefficients for Reactions of the Ethynyl Radical (C_2H) with C_3H_4 Isomers Methylacetylene and Allene. *J. Phys. Chem. A* **1999**, *103*, 1342–1346.
- (3) Huang, L. C. L.; Asvany, O.; Chang, A. H. H.; Balucani, N.; Lin, S. H.; Lee, Y. T.; Kaiser, R. I. Crossed Beam Reaction of Cyano Radicals with Hydrocarbon Molecules. IV. Chemical Dynamics of Cyanoacetylene (HCCCN; $X^1\Sigma^+$) Formation from Reaction of CN($X^2\Sigma^+$) with Acetylene, $C_2H_2(X^1\Sigma_g^+)$. *J. Chem. Phys.* **2000**, *113*, 8656–8666.
- (4) Balucani, N.; Asvany, O.; Chang, A. H. H.; Lin, S. H.; Lee, Y. T.; Kaiser, R. I.; Osamura, Y. Crossed Beam Reaction of Cyano Radicals with Hydrocarbon Molecules. III. Chemical Dynamics of Vinylcyanide (C_2H_3CN ; X^1A') Formation from Reaction of CN($X^2\Sigma^+$) with Ethylene, $C_2H_4(X^1A_g)$. *J. Chem. Phys.* **2000**, *113*, 8643–8655.
- (5) Balucani, N.; Asvany, O.; Chang, A. H. H.; Lin, S. H.; Lee, Y. T.; Kaiser, R. I.; Bettinger, H. F.; Schleyer, P. v. R.; Schaefer, H. F., III. Crossed Beam Reaction of Cyano Radicals with Hydrocarbon Molecules. I. Chemical Dynamics of Cyanobenzene (C_6H_5CN ; X^1A_1) and Perdeutero Cyanobenzene (C_6D_5CN ; X^1A_1) Formation from Reaction of CN($X^2\Sigma^+$) with Benzene $C_6H_6(X^1A_{1g})$, and de-Benzene $C_6D_6(X^1A_{1g})$. *J. Chem. Phys.* **1999**, *111*, 7457–7471.
- (6) Balucani, N.; Asvany, O.; Kaiser, R. I.; Osamura, Y. Formation of Three C_4H_3N Isomers from the Reaction of CN($X^2\Sigma^+$) with Allene, $H_2CCCH_2(X^1A_1)$, and Methylacetylene, CH_3CCH (X^1A_1): A Combined Crossed Beam and Ab Initio Study. *J. Phys. Chem. A* **2002**, *106*, 4301–4311.
- (7) Huang, L. C. L.; Balucani, N.; Lee, Y. T.; Kaiser, R. I.; Osamura, Y. Crossed Beam Reaction of the Cyano Radical, CN($X^2\Sigma^+$), with Methylacetylene, CH_3CCH (X^1A_1): Observation of Cyanopropyne, CH_3CCCN (X^1A_1), and Cyanoallene, $H_2CCCHCN$ (X^1A'). *J. Chem. Phys.* **1999**, *111*, 2857–2860.
- (8) Gu, X. B.; Zhang, F. T.; Kaiser, R. I. Reaction Dynamics on the Formation of 1- and 3-Cyanopropylene in the Crossed Beams Reaction of Ground-State Cyano Radicals (CN) with Propylene (C_3H_6) and Its Deuterated Isotopologues. *J. Phys. Chem. A* **2008**, *112*, 9607–9613.
- (9) Huang, C. H.; Kaiser, R. I.; Chang, A. H. H. Theoretical Study on the Reaction of Ground State Cyano Radical with Propylene in Titan's Atmosphere. *J. Phys. Chem. A* **2009**, *113*, 12675–12685.
- (10) Rhee, Y. M.; Lee, T. J.; Gudipati, M. S.; Allamandola, L. J.; Head-Gordon, M. Charged Polycyclic Aromatic Hydrocarbon Clusters and the Galactic Extended Red Emission. *Proc. Natl. Acad. Sci. U.S.A.* **2007**, *104*, 5274–5278.
- (11) Allamandola, L. J.; Tielens, A. G. G. M.; Barker, J. R. Polycyclic Aromatic Hydrocarbons and the Unidentified Infrared Emission Bands: Auto Exhaust along the Milky way! *Astrophys. J.* **1985**, *290*, L25–L28.
- (12) Salama, F.; Allamandola, L. J. Is A Pyrene-Like Molecular Ion the Cause of 4,430 Å Diffuse Interstellar Absorption Band? *Nature* **1992**, *358*, 42–43.
- (13) Cernicharo, J.; Heras, A. M.; Tielens, A. G. G. M.; Pardo, J. R.; Herpin, F.; Guélin, M.; Waters, L. B. F. M. Infrared Space Observatory's Discovery of C_4H_2 , C_6H_2 , and Benzene in CRL 618. *Astrophys. J.* **2001**, *546*, L123–L126.
- (14) Jones, B. M.; Zhang, F. T.; Kaiser, R. I.; Jamal, A.; Mebel, A. M.; Cordiner, M. A.; Charnley, S. B. Formation of Benzene in the Interstellar Medium. *Proc. Natl. Acad. Sci. U.S.A.* **2011**, *108*, 452–457.
- (15) Morales, S. B.; Bennett, C. J.; Le Picard, S. D.; Canosa, A.; Sims, I. R.; Sun, B. J.; Chen, P. H.; Chang, A. H. H.; Kislov, V. V.; Mebel, A. M.; et al. A Crossed Molecular Beam, Low-Temperature Kinetics, and Theoretical Investigation of the Reaction of the Cyano Radical (CN) with 1,3-Butadiene (C_4H_6). A Route to Complex Nitrogen-Bearing Molecules in Low-Temperature Extraterrestrial Environments. *Astrophys. J.* **2011**, *742*, 26.
- (16) Sun, B. J.; Huang, C. Y.; Kuo, H. H.; Chen, K. T.; Sun, H. L.; Huang, C. H.; Tsai, M. F.; Kao, C. H.; Wang, Y. S.; Gao, L. G.; et al. Formation of Interstellar 2,4-Pentadiynylidyne, $HCCCC(X_2\Pi)$, via the Neutral-Neutral Reaction of Ground State Carbon Atom, $C(^3P)$, with Diacetylene, $HCCCCH(X^1\Sigma_g^+)$. *J. Chem. Phys.* **2008**, *128*, 244303.
- (17) Sun, B. J.; Huang, C. H.; Tsai, M. F.; Sun, H. L.; Gao, L. G.; Wang, Y. S.; Yeh, Y. Y.; Shih, Y. H.; Sia, Z. F.; Chen, P. H.; et al. Synthesis of Interstellar 1,3,5-heptatriynylidyne, $C_7H(X^2\Pi)$, via the Neutral-Neutral Reaction of Ground State Carbon Atom, $C(^3P)$, with Triacetylene, $HC_6H(X^1\Sigma_g^+)$. *J. Chem. Phys.* **2009**, *131*, 104305.
- (18) Becke, A. D. Density-Functional Thermochemistry. III. The Role of Exact Exchange. *J. Chem. Phys.* **1993**, *98*, 5648–5652.
- (19) Becke, A. D. Density-Functional Thermochemistry. I. The Effect of the Exchange-Only Gradient Correction. *J. Chem. Phys.* **1992**, *96*, 2155–2160.
- (20) Becke, A. D. Density-Functional Thermochemistry. II. The Effect of the Perdew–Wang Generalized-Gradient Correlation Correction. *J. Chem. Phys.* **1992**, *97*, 9173–9177.
- (21) Lee, C.; Yang, W.; Parr, R. G. Development of the Colle-Salvetti Correlation-Energy Formula into a Functional of the Electron Density. *Phys. Rev. B* **1988**, *37*, 785–789.
- (22) Purvis, G. D.; Bartlett, R. J. A Full Coupled-Cluster Singles and Doubles Model: The Inclusion of Disconnected Triples. *J. Chem. Phys.* **1982**, *76*, 1910–1918.
- (23) Hampel, C.; Peterson, K. A.; Werner, H.-J. A Comparison of the Efficiency and Accuracy of the Quadratic Configuration Interaction (QCISD), Coupled Cluster (CCSD), and Brueckner Coupled Cluster (BCCD) Methods. *Chem. Phys. Lett.* **1992**, *190*, 1–12.
- (24) Knowles, P. J.; Hampel, C.; Werner, H.-J. Coupled Cluster Theory for High Spin, Open Shell Reference Wave Functions. *J. Chem. Phys.* **1993**, *99*, 5219–5227.
- (25) Deegan, M. J. O.; Knowles, P. J. Perturbative Corrections to Account for Triple Excitations in Closed and Open Shell Coupled Cluster Theories. *Chem. Phys. Lett.* **1994**, *227*, 321–326.
- (26) Frisch, M. J.; Trucks, G. W.; Schlegel, H. B. et al. *Gaussian* 98, revision A.5; Gaussian, Inc.: Pittsburgh, PA, 1998; *Gaussian* 03, Revision C.02; Gaussian, Inc.: Wallingford, CT, 2004.
- (27) Eyring, H.; Lin, S. H.; Lin, S. M. *Basic Chemical Kinetics*; Wiley: New York, 1980.
- (28) Chang, A. H. H.; Mebel, A. M.; Yang, X. M.; Lin, S. H.; Lee, Y. T. Ab initio/RKRM Approach Toward the Understanding of Ethylene Photodissociation. *J. Chem. Phys.* **1998**, *109*, 2748–2761.
- (29) Estillor, A. D.; Visger, L. M.; Kaiser, R. I.; Suits, A. G. Crossed-Beam Imaging of the H Abstraction Channel in the Reaction of CN with 1-Pentene. *J. Phys. Chem. Lett.* **2010**, *1*, 2417–2421.